DESY 96-163
August 1996

ISSN 0418-9833

Search for Excited Fermions with the H1 Detector

H1 Collaboration

Abstract:

We present a search for excited electrons, neutrinos and quarks using the H1 detector at the *ep* collider HERA, based on data taken in 1994 with an integrated luminosity of 2.75 pb^{-1}. Radiative decays of excited quarks and neutrinos have been investigated as well as decays of excited electrons into all possible electroweak gauge bosons. No evidence for new particle production is found and exclusion limits are derived.

S. Aid[13], M. Anderson[23], V. Andreev[26], B. Andrieu[29], A. Babaev[25], J. Bähr[36], J. Bán[18], Y. Ban[28], P. Baranov[26], E. Barrelet[30], R. Barschke[11], W. Bartel[11], M. Barth[4], U. Bassler[30], H.P. Beck[38], M. Beck[14], H.-J. Behrend[11], A. Belousov[26], Ch. Berger[1], G. Bernardi[30], G. Bertrand-Coremans[4], M. Besançon[9], R. Beyer[11], P. Biddulph[23], P. Bispham[23], J.C. Bizot[28], V. Blobel[13], K. Borras[8], V. Boudry[29], A. Braemer[15], W. Braunschweig[1], V. Brisson[28], W. Brückner[14], P. Bruel[29], D. Bruncko[18], C. Brune[16], R. Buchholz[11], L. Büngener[13], J. Bürger[11], F.W. Büsser[13], A. Buniatian[4,39], S. Burke[19], M.J. Burton[23], D. Calvet[24], A.J. Campbell[11], T. Carli[27], M. Charlet[11], D. Clarke[5], A.B. Clegg[19], B. Clerbaux[4], S. Cocks[20], J.G. Contreras[8], C. Cormack[20], J.A. Coughlan[5], A. Courau[28], M.-C. Cousinou[24], G. Cozzika[9], L. Criegee[11], D.G. Cussans[5], J. Cvach[31], S. Dagoret[30], J.B. Dainton[20], W.D. Dau[17], K. Daum[42], M. David[9], C.L. Davis[19], B. Delcourt[28], A. De Roeck[11], E.A. De Wolf[4], M. Dirkmann[8], P. Dixon[19], P. Di Nezza[33], W. Dlugosz[7], C. Dollfus[38], K.T. Donovan[21], J.D. Dowell[3], H.B. Dreis[2], A. Droutskoi[25], O. Dünger[13], H. Duhm[12,†] J. Ebert[35], T.R. Ebert[20], G. Eckerlin[11], V. Efremenko[25], S. Egli[38], R. Eichler[37], F. Eisele[15], E. Eisenhandler[21], E. Elsen[11], M. Erdmann[15], W. Erdmann[37], A.B. Fahr[13], L. Favart[28], A. Fedotov[25], R. Felst[11], J. Feltesse[9], J. Ferencei[18], F. Ferrarotto[33], K. Flamm[11], M. Fleischer[8], M. Flieser[27], G. Flügge[2], A. Fomenko[26], J. Formánek[32], J.M. Foster[23], G. Franke[11], E. Fretwurst[12], E. Gabathuler[20], K. Gabathuler[34], F. Gaede[27], J. Garvey[3], J. Gayler[11], M. Gebauer[36], H. Genzel[1], R. Gerhards[11], A. Glazov[36], L. Goerlich[6], N. Gogitidze[26], M. Goldberg[30], D. Goldner[8], K. Golec-Biernat[6], B. Gonzalez-Pineiro[30], I. Gorelov[25], C. Grab[37], H. Grässler[2], T. Greenshaw[20], R.K. Griffiths[21], G. Grindhammer[27], A. Gruber[27], C. Gruber[17], T. Hadig[1], D. Haidt[11], L. Hajduk[6], T. Haller[14], M. Hampel[1], W.J. Haynes[5], B. Heinemann[13], G. Heinzelmann[13], R.C.W. Henderson[19], H. Henschel[36], I. Herynek[31], M.F. Hess[27], K. Hewitt[3], W. Hildesheim[11], K.H. Hiller[36], C.D. Hilton[23], J. Hladký[31], M. Höppner[8], D. Hoffmann[11], T. Holtom[20], R. Horisberger[34], V.L. Hudgson[3], M. Hütte[8], M. Ibbotson[23], H. Itterbeck[1], A. Jacholkowska[28], C. Jacobsson[22], M. Jaffre[28], J. Janoth[16], D.M. Jansen[14], T. Jansen[11], L. Jönsson[22], D.P. Johnson[4], H. Jung[22], P.I.P. Kalmus[21], M. Kander[11], D. Kant[21], R. Kaschowitz[2], U. Kathage[17], J. Katzy[15], H.H. Kaufmann[36], O. Kaufmann[15], M. Kausch[11], S. Kazarian[11], I.R. Kenyon[3], S. Kermiche[24], C. Keuker[1], C. Kiesling[27], M. Klein[36], C. Kleinwort[11], G. Knies[11], T. Köhler[1], J.H. Köhne[27], H. Kolanoski[36,41], S.D. Kolya[23], V. Korbel[11], P. Kostka[36], S.K. Kotelnikov[26], T. Krämerkämper[8], M.W. Krasny[6,30], H. Krehbiel[11], D. Krücker[27], H. Küster[22], M. Kuhlen[27], T. Kurča[36], J. Kurzhöfer[8], D. Lacour[30], B. Laforge[9], M.P.J. Landon[21], W. Lange[36], U. Langenegger[37], A. Lebedev[26], F. Lehner[11], S. Levonian[29], G. Lindström[12], M. Lindstroem[22], F. Linsel[11], J. Lipinski[13], B. List[11], G. Lobo[28], P. Loch[11,43], J.W. Lomas[23], G.C. Lopez[12], V. Lubimov[25], D. Lüke[8,11], L. Lytkin[14], N. Magnussen[35], E. Malinovski[26], R. Maraček[18], P. Marage[4], J. Marks[24], R. Marshall[23], J. Martens[35], G. Martin[13], R. Martin[20], H.-U. Martyn[1], J. Martyniak[6], T. Mavroidis[21], S.J. Maxfield[20], S.J. McMahon[20], A. Mehta[5], K. Meier[16], F. Metlica[14], A. Meyer[11], A. Meyer[13], H. Meyer[35], J. Meyer[11], P.-O. Meyer[2], A. Migliori[29], S. Mikocki[6], D. Milstead[20], J. Moeck[27], F. Moreau[29], J.V. Morris[5], E. Mroczko[6], D. Müller[38], G. Müller[11], K. Müller[11], P. Murín[18], V. Nagovizin[25], R. Nahnhauer[36], B. Naroska[13], Th. Naumann[36], I. Négri[24], P.R. Newman[3], D. Newton[19], H.K. Nguyen[30], T.C. Nicholls[3], F. Niebergall[13], C. Niebuhr[11], Ch. Niedzballa[1], H. Niggli[37], G. Nowak[6], G.W. Noyes[5], T. Nunnemann[14], M. Nyberg-Werther[22], M. Oakden[20], H. Oberlack[27], J.E. Olsson[11], D. Ozerov[25], P. Palmen[2], E. Panaro[11], A. Panitch[4], C. Pascaud[28], G.D. Patel[20], H. Pawletta[2], E. Peppel[36], E. Perez[9], J.P. Phillips[20], A. Pieuchot[24], D. Pitzl[37], G. Pope[7], B. Povh[14], S. Prell[11], K. Rabbertz[1], G. Rädel[11], P. Reimer[31], S. Reinshagen[11], H. Rick[8], F. Riepenhausen[2], S. Riess[13], E. Rizvi[21], S.M. Robertson[3], P. Robmann[38], H.E. Roloff[36,†], R. Roosen[4], K. Rosenbauer[1], A. Rostovtsev[25], F. Rouse[7], C. Royon[9], K. Rüter[27], S. Rusakov[26], K. Rybicki[6], D.P.C. Sankey[5], P. Schacht[27], S. Schiek[13], S. Schleif[16], P. Schleper[15], W. von Schlippe[21], D. Schmidt[35], G. Schmidt[13], A. Schöning[11], V. Schröder[11], E. Schuhmann[27], B. Schwab[15], F. Sefkow[38], R. Sell[11], A. Semenov[25], V. Shekelyan[11],

I. Sheviakov[26], L.N. Shtarkov[26], G. Siegmon[17], U. Siewert[17], Y. Sirois[29], I.O. Skillicorn[10], P. Smirnov[26], V. Solochenko[25], Y. Soloviev[26], A. Specka[29], J. Spiekermann[8], S. Spielman[29], H. Spitzer[13], F. Squinabol[28], P. Steffen[11], R. Steinberg[2], H. Steiner[11,40], J. Steinhart[13], B. Stella[33], A. Stellberger[16], J. Stier[11], J. Stiewe[16], U. Stößlein[36], K. Stolze[36], U. Straumann[15], W. Struczinski[2], J.P. Sutton[3], S. Tapprogge[16], M. Taševský[32], V. Tchernyshov[25], S. Tchetchelnitski[25], J. Theissen[2], C. Thiebaux[29], G. Thompson[21], R. Todenhagen[14], P. Truöl[38], G. Tsipolitis[37], J. Turnau[6], J. Tutas[15], E. Tzamariudaki[11], P. Uelkes[2], A. Usik[26], S. Valkár[32], A. Valkárová[32], C. Vallée[24], D. Vandenplas[29], P. Van Esch[4], P. Van Mechelen[4], Y. Vazdik[26], P. Verrecchia[9], G. Villet[9], K. Wacker[8], A. Wagener[2], M. Wagener[34], B. Waugh[23], G. Weber[13], M. Weber[16], D. Wegener[8], A. Wegner[27], T. Wengler[15], M. Werner[15], L.R. West[3], T. Wilksen[11], S. Willard[7], M. Winde[36], G.-G. Winter[11], C. Wittek[13], M. Wobisch[2], E. Wünsch[11], J. Žáček[32], D. Zarbock[12], Z. Zhang[28], A. Zhokin[25], P. Zini[30], F. Zomer[28], J. Zsembery[9], K. Zuber[16], and M. zurNedden[38]

[1] *I. Physikalisches Institut der RWTH, Aachen, Germany*[a]
[2] *III. Physikalisches Institut der RWTH, Aachen, Germany*[a]
[3] *School of Physics and Space Research, University of Birmingham, Birmingham, UK*[b]
[4] *Inter-University Institute for High Energies ULB-VUB, Brussels; Universitaire Instelling Antwerpen, Wilrijk; Belgium*[c]
[5] *Rutherford Appleton Laboratory, Chilton, Didcot, UK*[b]
[6] *Institute for Nuclear Physics, Cracow, Poland*[d]
[7] *Physics Department and IIRPA, University of California, Davis, California, USA*[e]
[8] *Institut für Physik, Universität Dortmund, Dortmund, Germany*[a]
[9] *CEA, DSM/DAPNIA, CE-Saclay, Gif-sur-Yvette, France*
[10] *Department of Physics and Astronomy, University of Glasgow, Glasgow, UK*[b]
[11] *DESY, Hamburg, Germany*[a]
[12] *I. Institut für Experimentalphysik, Universität Hamburg, Hamburg, Germany*[a]
[13] *II. Institut für Experimentalphysik, Universität Hamburg, Hamburg, Germany*[a]
[14] *Max-Planck-Institut für Kernphysik, Heidelberg, Germany*[a]
[15] *Physikalisches Institut, Universität Heidelberg, Heidelberg, Germany*[a]
[16] *Institut für Hochenergiephysik, Universität Heidelberg, Heidelberg, Germany*[a]
[17] *Institut für Reine und Angewandte Kernphysik, Universität Kiel, Kiel, Germany*[a]
[18] *Institute of Experimental Physics, Slovak Academy of Sciences, Košice, Slovak Republic*[f,j]
[19] *School of Physics and Chemistry, University of Lancaster, Lancaster, UK*[b]
[20] *Department of Physics, University of Liverpool, Liverpool, UK*[b]
[21] *Queen Mary and Westfield College, London, UK*[b]
[22] *Physics Department, University of Lund, Lund, Sweden*[g]
[23] *Physics Department, University of Manchester, Manchester, UK*[b]
[24] *CPPM, Université d'Aix-Marseille II, IN2P3-CNRS, Marseille, France*
[25] *Institute for Theoretical and Experimental Physics, Moscow, Russia*
[26] *Lebedev Physical Institute, Moscow, Russia*[f]
[27] *Max-Planck-Institut für Physik, München, Germany*[a]
[28] *LAL, Université de Paris-Sud, IN2P3-CNRS, Orsay, France*
[29] *LPNHE, Ecole Polytechnique, IN2P3-CNRS, Palaiseau, France*
[30] *LPNHE, Universités Paris VI and VII, IN2P3-CNRS, Paris, France*
[31] *Institute of Physics, Czech Academy of Sciences, Praha, Czech Republic*[f,h]
[32] *Nuclear Center, Charles University, Praha, Czech Republic*[f,h]
[33] *INFN Roma 1 and Dipartimento di Fisica, Università Roma 3, Roma, Italy*
[34] *Paul Scherrer Institut, Villigen, Switzerland*
[35] *Fachbereich Physik, Bergische Universität Gesamthochschule Wuppertal, Wuppertal, Germany*[a]
[36] *DESY, Institut für Hochenergiephysik, Zeuthen, Germany*[a]

[37] *Institut für Teilchenphysik, ETH, Zürich, Switzerland*[i]
[38] *Physik-Institut der Universität Zürich, Zürich, Switzerland*[i]
[39] *Visitor from Yerevan Phys. Inst., Armenia*
[40] *On leave from LBL, Berkeley, USA*
[41] *Institut für Physik, Humboldt-Universität, Berlin, Germany*[a]
[42] *Rechenzentrum, Bergische Universität Gesamthochschule Wuppertal, Wuppertal, Germany*[a]
[43] *Physics Department, University of Arizona, Tuscon, USA*

† *Deceased*

[a] *Supported by the Bundesministerium für Bildung, Wissenschaft, Forschung und Technologie, FRG, under contract numbers 6AC17P, 6AC47P, 6DO57I, 6HH17P, 6HH27I, 6HD17I, 6HD27I, 6KI17P, 6MP17I, and 6WT87P*
[b] *Supported by the UK Particle Physics and Astronomy Research Council, and formerly by the UK Science and Engineering Research Council*
[c] *Supported by FNRS-NFWO, IISN-IIKW*
[d] *Supported by the Polish State Committee for Scientific Research, grant nos. 115/E-743/SPUB/P03/109/95 and 2 P03B 244 08p01, and Stiftung für Deutsch-Polnische Zusammenarbeit, project no. 506/92*
[e] *Supported in part by USDOE grant DE F603 91ER40674*
[f] *Supported by the Deutsche Forschungsgemeinschaft*
[g] *Supported by the Swedish Natural Science Research Council*
[h] *Supported by GA ČR grant no. 202/93/2423, GA AV ČR grant no. 19095 and GA UK grant no. 342*
[i] *Supported by the Swiss National Science Foundation*
[j] *Supported by VEGA SR grant no. 2/1325/96*

1 Introduction

In composite models of quarks and leptons it is natural to expect new heavy particles, which can be interpreted as excitations of the ground state. The direct observation of either excited leptons or excited quarks would certainly provide strong evidence for a new layer in the substructure of matter.

Electron proton interactions at very high energies provide an excellent environment to look for excited leptons and quarks. If we consider for example excited electrons, these states can only be reached via magnetic type couplings [1] because the electromagnetic current is conserved in electromagnetic interactions. It has been shown [2], that about half of the cross section is expected in the elastic channel

$$e + p \rightarrow e^* + p \tag{1}$$

with a branching ratio of e.g. 30% [3] into $e\gamma$ for the decay of an e^* with a mass of more than 150 GeV. This reaction has an extremely clear signature, a wide angle electron photon pair and nothing else in the detector. The analysis of other decay channels (e.g. $e^* \rightarrow e + jets$) or of inelastically produced excited electrons ($e + p \rightarrow e^* + X$) is more complicated. The present paper covers elastic and inelastic e^* production in all decay channels.

The magnetic coupling can also be applied to other gauge boson interactions. Excited neutrinos could for example be produced in charged current reactions, $e + p \rightarrow \nu^* + X$. The ν^* will decay into $\nu\gamma, \nu Z$ or νW. This analysis considers a search for $e + p \rightarrow \nu^* + X, \nu^* \rightarrow \nu + \gamma$ because of the clear signature of this particular decay channel and because theoretical models [3] can be constructed which predict a high branching ratio BR^* of $\nu^* \rightarrow \nu\gamma$.

In the same way the magnetic transition coupling of quarks would allow single production of excited quarks through t-channel gauge boson exchange between the incoming electrons and quarks. The cross section is dominated by γ exchange with very small values of the squared momentum transfer (photoproduction limit) and therefore the scattered electron is unseen in the detector. The decay $q^* \rightarrow q + \gamma$ again provides a clear signature and a search for this channel is also described in this paper.

The essential parameter in the production and decay of excited fermions (f^*) of mass M is the partial width $\Gamma(f^* \rightarrow fV)$, where V represents a heavy boson (W, Z) or photon. In the photonic case this partial width is given by

$$\Gamma(f^* \rightarrow f\gamma) = \frac{\alpha M^3 c^2_{\gamma f^* f}}{\Lambda^2} \quad . \tag{2}$$

A general treatment can be found in ref. [3]. The couplings c_{Vf^*f} are a priori unknown. The theoretical calculation is model dependent, see for example [3]. The parameter Λ determines the compositeness scale. It is presently constrained to values above 0.7 to 1 TeV.

In the narrow width approximation the total cross section for elastic production of excited electrons is given by

$$\sigma(ep \rightarrow e^*p) = \frac{4\pi^2}{s}(2J+1)\frac{\Gamma}{M} f_{\gamma/p}(M^2/s) \tag{3}$$

where J is the spin of the new fermion and $\sqrt{s}$ the center of mass energy ($\approx$ 300 GeV at HERA). The number of photons with momentum fraction between z and $z + dz$ radiated off the proton is given by $f_{\gamma/p}(z)$. It can be evaluated using e.g. the formula given in ref. [4]. In the case of excited quark production the relevant formula includes a convolution of the photon densities $f_{\gamma/e}$ in the electron and the quark densities $f_{q/p}$ in the proton. More general expressions for e^* and ν^* production are given in ref. [2]. Because the calculation of the widht, Γ, and the branching ratio, BR^*, for the decay of the new fermion into a specific final state are model dependent,

the experimental exclusion limits obtained in this paper are quoted for the products $\sigma \cdot BR^*$. They can therefore also be used as exclusion limits for arbitrary heavy objects decaying into the investigated final states.

Although most models would expect excited states with masses of the order of the compositeness scale it is important to cover experimentally the $M < 300$ GeV region accessible for direct searches at HERA. This analysis uses data taken with the H1 detector in 1994 at HERA with an integrated luminosity of 2.75 pb^{-1} in positron proton collisions[1] at a center of mass energy of 300 GeV. Previous searches for excited fermions made with the H1-detector are described in ref.s [5] and [6]. A similar search has been presented by the ZEUS collaboration [7].

2 Experimental set-up

A detailed description of the H1 detector can be found elsewhere [8]. Here we describe briefly the components which are relevant for this analysis. The interaction region is surrounded by a drift and proportional chamber tracking system, split into central barrel and forward parts and covering the angular range $7° \leq \theta \leq 176°$ [2]. The tracking system is placed inside a finely segmented liquid argon (LAr) calorimeter covering the range $4° \leq \theta \leq 153°$. The electromagnetic section, between 20 and 30 radiation lengths (X_0) deep, is used to identify electrons and photons. Hadrons also deposit energy in the outer layers (hadronic section) of the LAr calorimeter. The total thickness of the LAr components varies between 4.5 and 8 interaction lengths. For the LAr calorimeter energy resolutions of $\sigma(E)/E \simeq 12\ \%/\sqrt{E\,(\mathrm{GeV})} \oplus 1\%$ for electrons and $\sigma(E)/E \simeq 50\ \%/\sqrt{E\,(\mathrm{GeV})} \oplus 2\%$ for hadrons have been obtained in test beam measurements. A 22 X_0 deep lead-scintillator electromagnetic calorimeter (BEMC) is located in the backward region ($151° \leq \theta \leq 176°$) of the H1 detector. The resolution is determined to be $\sigma(E)/E \simeq 10\ \%/\sqrt{E\,(\mathrm{GeV})} \oplus 2\%$.

The tracking system and calorimeters are surrounded by a super-conducting solenoid producing a uniform field of 1.15 T in the z-direction. The iron return yoke of the main solenoid is instrumented with limited streamer tubes to measure tracks of penetrating muons in the range of polar angles $5° \leq \theta \leq 170°$. There is an additional forward muon spectrometer to measure high energy muons in the region $3° \leq \theta \leq 17°$.

The luminosity detectors, which measure the Bethe-Heitler reaction $ep \to e\gamma p$ and electrons from photoproduction processes, are placed at the positions $z = -33$ m (electron tagger) and at $z = -103$ m (photon tagger), measured along the direction of the proton beam with respect to the nominal interaction point.

3 Search for excited leptons

3.1 Exclusive electromagnetic cluster analysis

The first search method looks for $e\gamma$ pairs in an otherwise empty detector. Exotic candidates for this reaction are elastically produced e^*s decaying into an electron and a photon. Also included are the so called quasi-elastic reactions (e.g. $e + p \to e^* + \Delta^+$) where the decay products of the hadronic state remain in the beam pipe.

[1] Only for ν^* production the charge of the incoming lepton is relevant.

[2] The forward direction (positive z-coordinate) from which the polar angle, θ, is measured is the proton beam direction.

Events have been selected with only two electromagnetic clusters and little additional energy observed in the detector. The main background source stems from the Wide-Angle Bremsstrahlung (WAB) process $ep \to e\gamma p(X)$ with a well separated $e\,\gamma$ pair in the final state. The WAB process constitutes a kinematically indistinguishable background to e^* production. Optimizing the cuts for the selection of WAB events therefore also optimizes the efficiency for excited electrons decaying into $e + \gamma$.

Most of the WAB events are expected to have an $e\,\gamma$ system of low invariant mass with high momentum in the direction of the incoming electron. The system is boosted into the forward direction only for masses of the $e\,\gamma$ system above $2\,E$, where E is the energy of the incoming electron (27.5 GeV).

Another type of expected background is that due to the so called Two Photon ($\gamma\,\gamma$) process $ep \to eeep(X)$, where an electron positron pair is produced in addition to the scattered positron. If two of these three leptons are seen inside the detector and one of them has no reconstructed track, due to geometrical acceptance or chamber inefficiencies, the event could be misinterpreted as an $e\,\gamma$ candidate.

The cuts to select $e\,\gamma$ pairs are shown in table 1. The events are required to have satisfied the BEMC or LAr energy triggers. Trigger efficiencies have been studied using selected WAB events with one electromagnetic cluster in the BEMC and the other in the LAr calorimeter. The trigger efficiencies are $\approx 100\,\%$ for electromagnetic clusters with energies above 8 GeV in the BEMC, above 14 GeV in the LAr barrel region ($\theta > 20°$), and above 30 GeV in the LAr forward region ($\theta < 20°$). Parameterized trigger efficiencies were then folded into the Monte Carlo models for the simulation of e^* production.

1. ≥ 2 isolated e.m. clusters, $E_i > 2$ GeV for $i = e, \gamma$
2. $E_e + E_\gamma > 20$ GeV
3. $E_{total} - E_e - E_\gamma < 5$ GeV
4. $\lvert m(\theta_e, \theta_\gamma) - m \rvert < 2\,m$
5. $\lvert E_i(\theta_e, \theta_\gamma) - E_i \rvert < E_i$
6. $\theta_i < 170°$
7. $10° < \theta_e < 160°$ or $10° < \theta_\gamma < 160°$
8. $20 < (E - p_z)_{total} < 80$ GeV
9. $-30 <$ z-vertex$<$ 40 cm, if z-vertex is reconstructed
10. $m > 10$ GeV
11. Visual scan

Table 1: Selection requirements for the exclusive electromagnetic cluster analysis. Here m is the invariant mass of the $e\,\gamma$ system. The other quantities are explained in the text. If more than two isolated e.m. clusters are found, the two clusters fulfilling requirements 1 and 2 with the largest polar angles θ_i are used.

We define an electromagnetic cluster as one which has at least 90 % of its energy deposited in the electromagnetic part of the calorimeters and which is isolated. The isolation requirement is based on a geometric cone in terms of azimuthal angle ($\Delta\phi$) and pseudo-rapidity ($\Delta\eta$) differences with respect to the center of the cluster. If less than 10 % additional energy is found outside the cluster but within $R = \sqrt{\Delta\phi^2 + \Delta\eta^2} < 0.5$, the cluster is defined as isolated.

Requirement 2 takes into account that for most elastic and quasi-elastic WAB events at low $e\,\gamma$ masses the summed energy of the two clusters is given by the energy, E, of the initial electron. Requirement 3 rejects events with other particles in the final state and thus represents the 'empty detector' condition. Here E_{total} is the total energy deposited in the BEMC and LAr calorimeters.

Requirements 4 and 5 are loose cuts in order to ensure the proper kinematics: for exclusive e^* ($\rightarrow e\,\gamma$) production as well as for the elastic and quasi-elastic WAB background the kinematics of the process is over-constrained. Using the polar angles θ_e and θ_γ alone, the electron or photon energies $E_i(\theta_e, \theta_\gamma)$ or the mass $m(\theta_e, \theta_\gamma)$ of the $e\,\gamma$ system can be calculated. These quantities can then be compared to the measured energies, E_i, and to the fully reconstructed invariant mass, m, using the measured 4-vectors. Requirement 6 excludes a region where WAB background is especially large. Requirements 7 and 8 suppress background from low squared momentum transfer Neutral Current (NC) Deep Inelastic Scattering (DIS) and $\gamma\,p$ events, respectively. Requirement 9 suppresses events which are not due to positron proton collisions.

442 events have passed the selection criteria including a cut $m > 10$ GeV . These events were scanned visually. Cosmic ray induced events (29 events) and beam halo muon events (39 events) of complicated topology were identified and removed at this stage. 124 events did not satisfy the $e\gamma$ hypothesis, because they had tracks pointing to two clusters or tracks uncorrelated with the electromagnetic clusters. This latter class of events is not due to the WAB process as was confirmed by a scan of WAB Monte Carlo events [9] corresponding to an integrated luminosity of 6 pb^{-1} . The same scanning procedure was also performed for selected Two Photon Monte Carlo events [10] (integrated luminosity of 9 pb^{-1}). The generated WAB and $\gamma\gamma$ events are processed using the H1 detector simulation program and are then subject to the same reconstruction and analysis procedures as the real data.

The remaining 250 events are compared to the WAB event simulation which predicts 257.2 ± 13.7 events (for an integrated luminosity of 2.75 pb^{-1}) and to the $\gamma\,\gamma$ event simulation, where 9.4 ± 1.6 events are expected.

The distributions of the energies and polar angles of the electromagnetic clusters (not shown) as well as the $e\,\gamma$ mass spectrum (figure 1) are reproduced well both in shape and absolute value by the WAB and $\gamma\gamma$ Monte Carlo simulations. Applying the Kolmogorov-Smirnov test [11] to the mass spectrum the probability is 90 % that both follow the same distribution. The highest measured mass is at 91.3 GeV. Above 50 GeV 4.6 events are expected and 4 events are seen. In total 0.6 events are expected from the WAB process for masses above 100 GeV.

3.2 Inclusive electromagnetic cluster analysis

Candidates for more general event topologies from heavy lepton decays, with two or more electromagnetic clusters as well as other particles in the final state, must fulfill the selection criteria shown in table 2. The selections in table 2 are motivated by Monte Carlo studies and will ensure high efficiencies for the high mass region in the channels $e^* \rightarrow e\,\gamma$ and $e^* \rightarrow e\,Z$, $Z \rightarrow e\,e$ for elastic and inelastic e^* production.

1. ≥ 2 isolated e.m. clusters, $E_{t1} > 20$ GeV, $E_{t2} > 10$ GeV
2. $20 < (E - p_z)_{total} < 80$ GeV
3. $-30 <$ z-vertex< 40 cm, if z-vertex is reconstructed
4. Visual scan

Table 2: Selection requirements for the inclusive electromagnetic cluster analysis. E_{t1} and E_{t2} are the transverse energies of the first and second cluster. If more than two isolated electromagnetic clusters are found, the two clusters with largest transverse energies are used.

328 events were selected and scanned visually and 65 cosmic muons and 167 beam halo muon events were removed from the data sample. First, the decay channel $e^* \rightarrow e\,\gamma$ was analyzed. 75 events are due to the DIS process where a hadronic jet near a ϕ-crack of the LAr calorimeter was

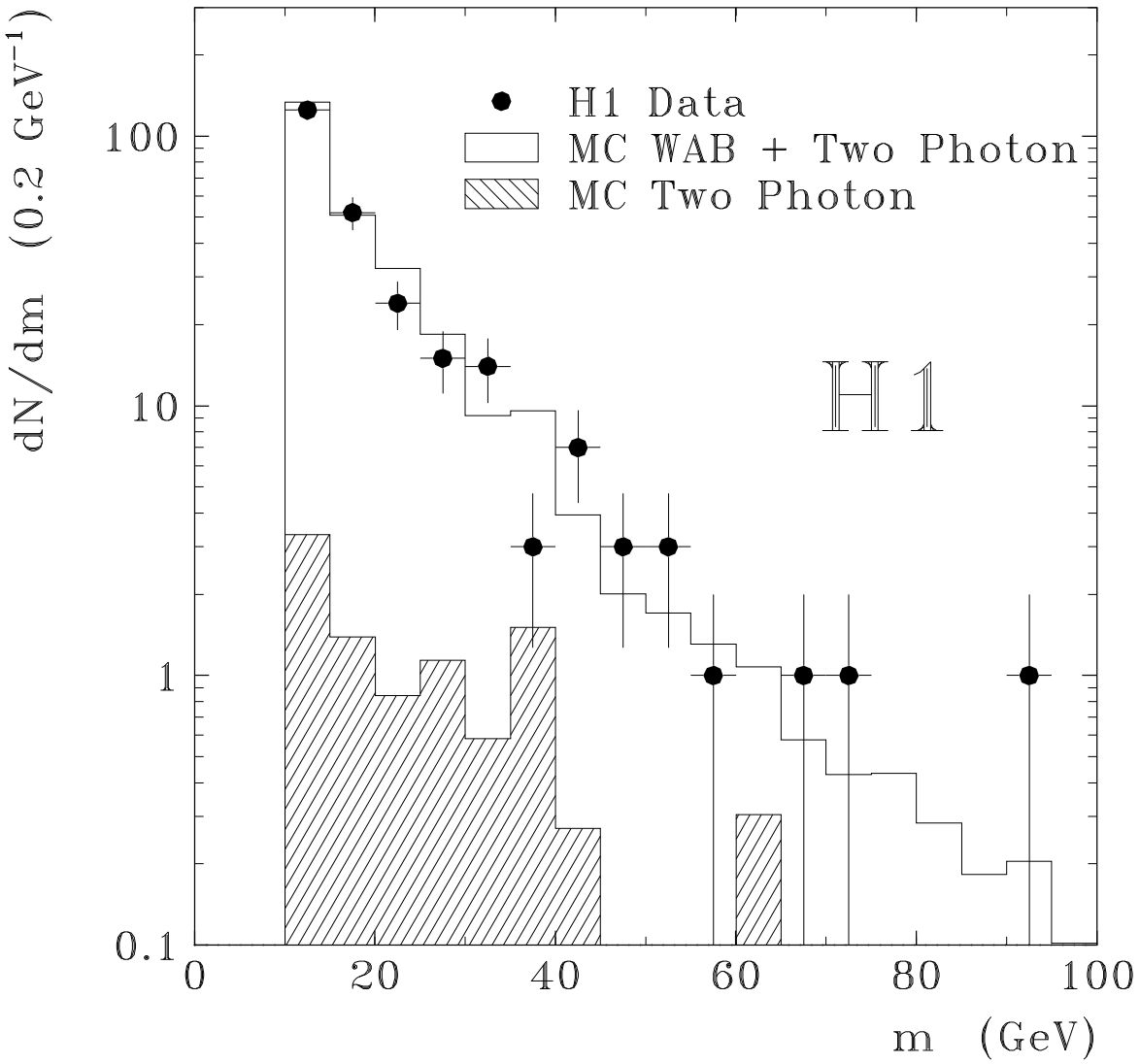

Figure 1: Mass spectrum of the selected $e\,\gamma$ pairs with masses above 10 GeV in the exclusive electromagnetic cluster analysis. Only statistical errors are shown. The shaded histogram shows the absolute prediction based on the Two Photon Monte Carlo simulation, and the open histogram shows the expectation for the sum of the Two Photon and WAB processes.

misidentified as an electromagnetic cluster. Two events are not considered as candidates for the $e\,\gamma$ final state as they have tracks pointing to both clusters. There remain 19 candidates for the decay channel $e^* \to e\,\gamma$ which are compared to the WAB [9] and NC DIS [12] event simulation. The expectations from these two processes are 10.8 ± 2.0 and 4.5 ± 1.3 events, respectively.

The absolute values and the shapes of the distributions for the transverse energies and polar angles of the electromagnetic clusters (not shown) as well as the invariant mass spectrum of the two clusters (figure 2) are reproduced well by the Monte Carlo simulation. Applying the Kolmogorov-Smirnov test to the mass spectra, the probability is 69 % that both follow the same distribution. The highest measured mass is at 154.3 GeV. In total 0.06 events are expected from the WAB process for masses above 150 GeV.

Candidates for the decay channel $e^* \to e\,Z$, $Z \to e\,e$ (21 events) must fulfill the following additional cuts: if there are exactly two isolated electromagnetic clusters in the event, both

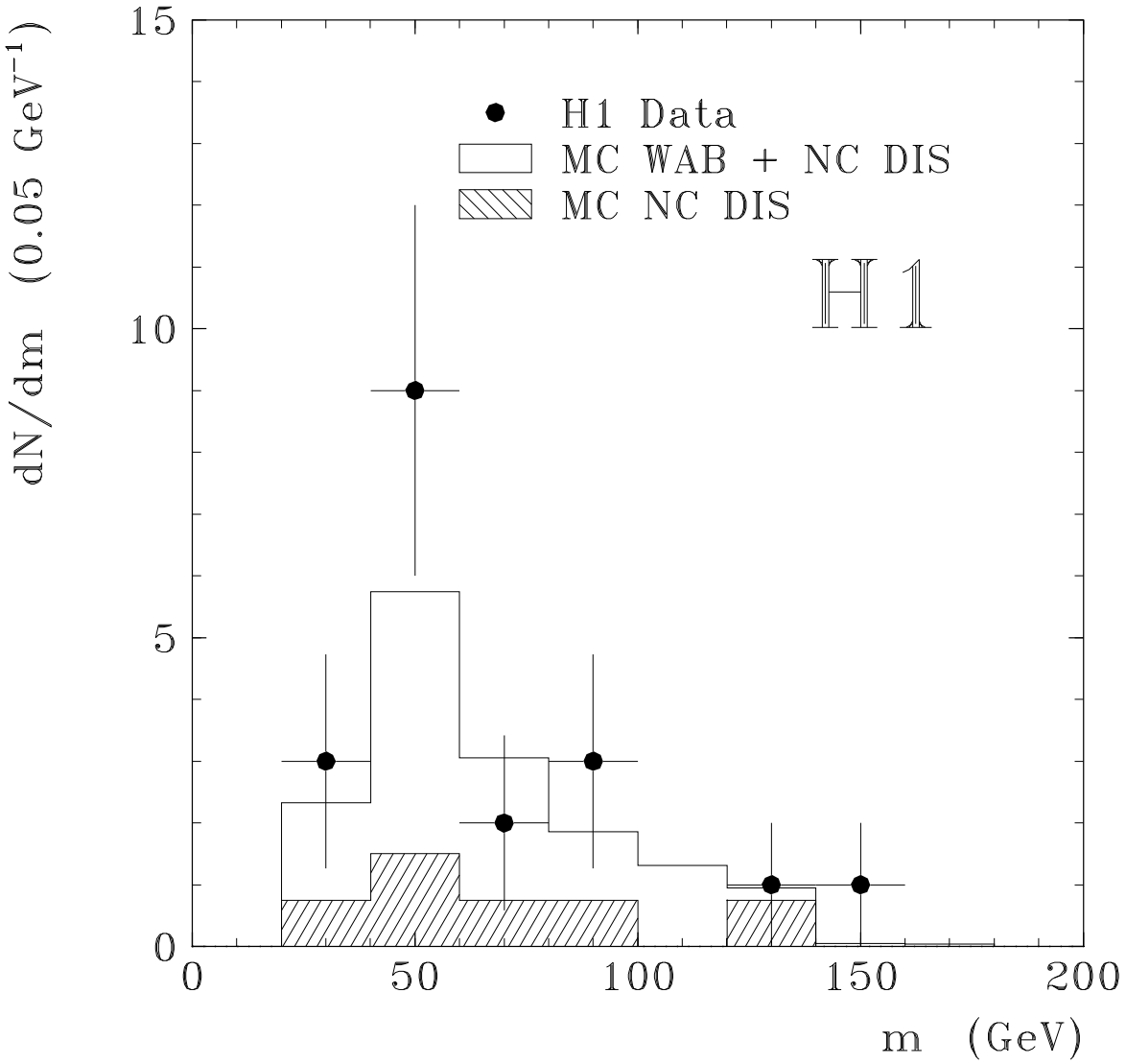

Figure 2: Mass spectrum of the selected high E_t electromagnetic cluster pairs in the inclusive electromagnetic cluster analysis. The shaded histogram shows the absolute prediction based on the DIS Monte Carlo simulation, and the open histogram shows the expectation for the sum of DIS and WAB reactions.

must have a polar angle, θ, above 20°. The invariant mass of the two cluster system must be between 80 GeV and 95 GeV. If more than two clusters are found, the third cluster must have $E_{t3} > 5$ GeV. The invariant mass, reconstructed from only two of the three clusters, which is nearest to the mass of the Z boson is then required to be between 80 GeV and 95 GeV.

These additional selections are applied to all 96 previously selected physics events (i.e. not cosmic or beam halo muon induced); no event survives and there are therefore no candidates left for this decay channel.

3.3 Cluster and missing transverse energy analysis

Events with at least one isolated high transverse energy electromagnetic cluster in addition to a large missing transverse energy are candidates for the decay channels $e^* \to e\,Z$, $Z \to$

$\nu\,\nu$, $e^* \to \nu\,W$, $W \to e\,\nu$, or $\nu^* \to \nu\,\gamma$ in both elastic and inelastic production processes. Background is expected from the NC DIS process with large fluctuations of missing transverse energy. Candidates for these event topologies must fulfill the selections shown in table 3.

Requirement 3 minimizes background from NC DIS reactions and enhances a possible signal with highly energetic neutrinos in the final state. Requirement 5, which excludes events with a muon track, serves as a simple cosmic and beam halo muon event filter.

1. ≥ 1 isolated electromagnetic cluster, $E_t > 20$ GeV
2. $E_t^{miss} > 20$ GeV
3. $(E - p_z)_{total} < 50$ GeV
4. $-30 < z$-vertex< 40 cm, z-vertex must be reconstructed
5. No rec. track in the instrumented iron with ≥ 8 hits
6. Visual scan

Table 3: Selection requirements for the electromagnetic cluster and missing transverse energy analysis. E_t is the transverse energy of the cluster, and E_t^{miss} is the total missing transverse energy of the event. If more than one isolated electromagnetic cluster is found, that with largest transverse energy is used.

268 events were selected and scanned visually and 111 cosmic events and 153 beam halo muon events were identified and removed at this stage. In one event a hadronic jet was misidentified as an electromagnetic cluster. Finally three candidate events remain, where 0.8 ± 0.5 events are expected from NC DIS [12] interactions.

For candidate events the 4-vector of the missing neutrino system, and therefore the invariant mass of the excited lepton, can be reconstructed for the decay channels $e^* \to e\,Z$, $Z \to \nu\,\nu$ and $\nu^* \to \nu\,\gamma$. For the channel $e^* \to \nu\,W$, $W \to e\,\nu$ the invariant mass of the two neutrinos was assumed to be that of the W-boson. This choice is a compromise and overestimates (underestimates) the reconstructed excited lepton mass in the low (high) mass region.

The reconstructed excited lepton masses of the three surviving events are 139 GeV, 148 GeV and 186 GeV for the hypothesis $e^* \to e\,Z$, $Z \to \nu\,\nu$, and 131 GeV, 134 GeV and 165 GeV assuming $e^* \to \nu\,W$, $W \to e\,\nu$. For both hypotheses no significant deviation in the mass distribution is observed compared to the NC DIS Monte Carlo simulation.

Events for the decay channel $\nu^* \to \nu\,\gamma$ are required to satisfy the additional requirement that there is no track with transverse momentum, p_t, above 5 GeV inside a cone of $R = 0.1$ in the η-ϕ-plane, centered around the isolated cluster, where R is defined as in the previous analysis (see section 3.1). None of the three data events survives this additional selection.

3.4 Inclusive muon analysis

Events with high transverse momentum (p_t) muons in the final state are selected as candidates for the decay channels $e^* \to e\,Z$, $Z \to \mu\,\mu$ and $e^* \to \nu\,W$, $W \to \mu\,\nu$ of elastically and inelastically produced excited leptons. High energy muon candidates in the final state are to be expected from the Two Photon process, $\gamma\,\gamma \to \mu\,\mu$, from photo- and electro-production of J/Ψ-mesons, from meson decays and from hadronic punch-through. The basic selection cuts are shown in table 4.

After applying the cuts 1–4 shown in table 4, 170 events remained and were visually scanned. Of these, 147 events were found to be cosmic or beam halo muons, leaving 16 single muon events,

1. ≥ 1 track in the instrumented iron
2. Link to a central vertex
3. $p_t > 10$ GeV of a central track linked to the iron track
4. Rejection of throughgoing cosmic ray muons
5. Visual scan
6.1 Second track in the instrumented iron, link to a central track
6.2 Invariant mass of two muon system greater than 60 GeV
7.1 No second track in the instrumented iron with link to a central track
7.2 ≤ 2 tracks beside muon track
7.3 No central track opposite in polar and azimuthal angle to the muon track

Table 4: Selection requirements for the inclusive muon analysis. p_t is the transverse momentum of the z-vertex fitted central track. Candidates for the decay channels $e^* \to e\,Z$, $Z \to \mu\,\mu$ or $e^* \to \nu\,W$, $W \to \mu\,\nu$ have to satisfy selection criteria 1–6 or 1–5 and 7, respectively.

6 two muon events, and one event with four muons in the final state. Applying the additional cuts 6.1 and 6.2 to select candidates for the decay channel $e^* \to e\,Z$, $Z \to \mu\,\mu$, no event remained. All masses of the two muon system are below 44 GeV and the events are therefore rejected. As well as the standard selection criteria 1–5 candidates for the decay channel $e^* \to \nu\,W$, $W \to \mu\,\nu$ have to satisfy the additional cuts 7.1–7.3. Only elastic e^* production is considered (cut 7.2) because it is difficult to identify single muons within jets. No event survives the cuts in this channel.

3.5 Jet analysis

In the context of this paper events with a final state including two or more jets with a high invariant mass are candidates for decays of the heavy gauge bosons W and Z. Background events are expected from photoproduction, NC DIS, or from Charged Current (CC) DIS processes. The cuts to select candidates for the decay channels $e^* \to e\,Z$, $Z \to q\,\bar{q}$ and $e^* \to \nu\,W$, $W \to q\,\bar{q}'$ are shown in table 5.

1. ≥ 2 jets, $E_{ti} > 15$ GeV, with $i = 1, 2$
2. $m_{12} > 60$ GeV
3. $E_{tag} < 2$ GeV
4. $-30 <$ z-vertex$<$ 40 cm, z-vertex must be reconstructed
5. Visual scan
6. Electron candidate, $\theta_e < 140°$
7.1 Reject events with an electron candidate
7.2 $E_t^{miss} > 20$ GeV
7.3 $(E - p_z)_{total} < 50$ GeV

Table 5: Selection requirements for the jet analysis. m_{12} is the invariant mass of the two jet system. If more than two jets are found, the two jets with highest transverse energies E_{ti} are used. E_{tag} is the energy deposited in the electron tagger. An electron candidate is defined as an isolated electromagnetic cluster with $E_e > 10$ GeV and $\theta_e > 10°$. The electron candidate with highest energy is ignored in the jet search.

A cone algorithm with radius $R = 1$ in the η-ϕ-plane is used to define jets. The two jets with largest transverse energies are used. If an electron candidate, defined as the most energetic

isolated electromagnetic cluster satisfying $E_e > 10$ GeV and $\theta_e > 10°$, is found, it is not included in the jet search. Requirement 3 rejects photoproduction events in which the scattered positron is detected in the electron tagger. Requirement 4 suppresses beam-gas events. The events are visually scanned and background events (cosmic muons) as well as events with misidentified electron candidates or jets are rejected. The same scanning procedure was also performed for Monte Carlo events.

The events were required to have a LAr transverse energy trigger. The efficiency of the LAr transverse energy trigger has been estimated using 55 events satisfying cuts 1, 2, 4, 5, and 7.1, which were triggered by the electron tagger. Of these events 51 also have a LAr transverse energy trigger, giving an efficiency of 93 %. If both jets have transverse energies, E_{ti}, greater than 20 GeV, the trigger efficiency rises to 100 %.

Candidates for the decay channel $e^* \to e\,Z$, $Z \to q\,\bar{q}$ are required to fulfill selection criteria 1–6. In this channel 15 data events are selected to be compared with the expected 14.6 ± 2.3 events from a NC DIS Monte Carlo simulation [12].

The absolute number of events as well as the invariant mass spectrum of the two jets and the electron, m_{12e}, (figure 3) are well reproduced by the Monte Carlo simulation. Applying the Kolmogorov-Smirnov test to the mass spectra (figure 3) the probability is 43 % that both follow the same distribution. The highest measured mass is at $m_{12e} = 164$ GeV.

Candidates for the second decay channel $e^* \to \nu\,W$, $W \to q\,\bar{q}'$ are required to fulfill selection criteria 1–5 and 7. Three data events survive the cuts compared with the 0.6 ± 0.6 events expected from a Monte Carlo simulation of photoproduction [13]. A rough estimate shows that from the CC DIS process approximately one further event is expected.

The invariant masses of the two jet system, m_{12}, for the three events are 73 GeV, 112 GeV, and 75 GeV respectively. The 4-vector of the missing neutrino is reconstructed and the invariant masses of the two jet system and the neutrino, $m_{12\nu}$ are found to be 120 GeV, 135 GeV, and 141 GeV respectively.

In summary, after imposing selection requirements for heavy gauge bosons, no significant excess of events is found in any of the channels under study. Where candidates still survive the cuts, their number is compatible with expectations from specific background processes.

3.6 Results of e^* and ν^* search

Table 6 shows the total efficiencies, including that of the trigger, for all excited lepton channels under study as a function of excited lepton mass. The Monte Carlo event generator COMPOS [14] based on the cross section calculated in ref. [2] is used. We employ the Lund string model [15] for hadronization and decays. All results presented here have been obtained using the MRS H [16] parameterization of the parton densities. The generated events are passed through the full H1 detector simulation and are reconstructed in the same manner as the real data.

The experiment can set limits on the product $\sigma \cdot BR^*$ of the production cross section with the branching ratio into a specific decay channel. The limits are derived by following the procedure recommended by the Particle Data Group [17]. Figure 4 shows the rejection limits at a 95 % Confidence Level (CL) for the e^* and ν^* as a function of the masses of the excited states. In calculating limits for the channel $e^* \to e\,\gamma$ both samples from the exclusive and the inclusive electromagnetic cluster analysis are combined as are the different decay channels of the W and Z heavy gauge bosons. The rejection limits for final states with a W or Z boson are similar, the main difference stemming from Z decays into $\nu\,\bar{\nu}$. The results improve earlier published H1 results [6] by a factor 3 to 6 in the limits for the excluded cross section.

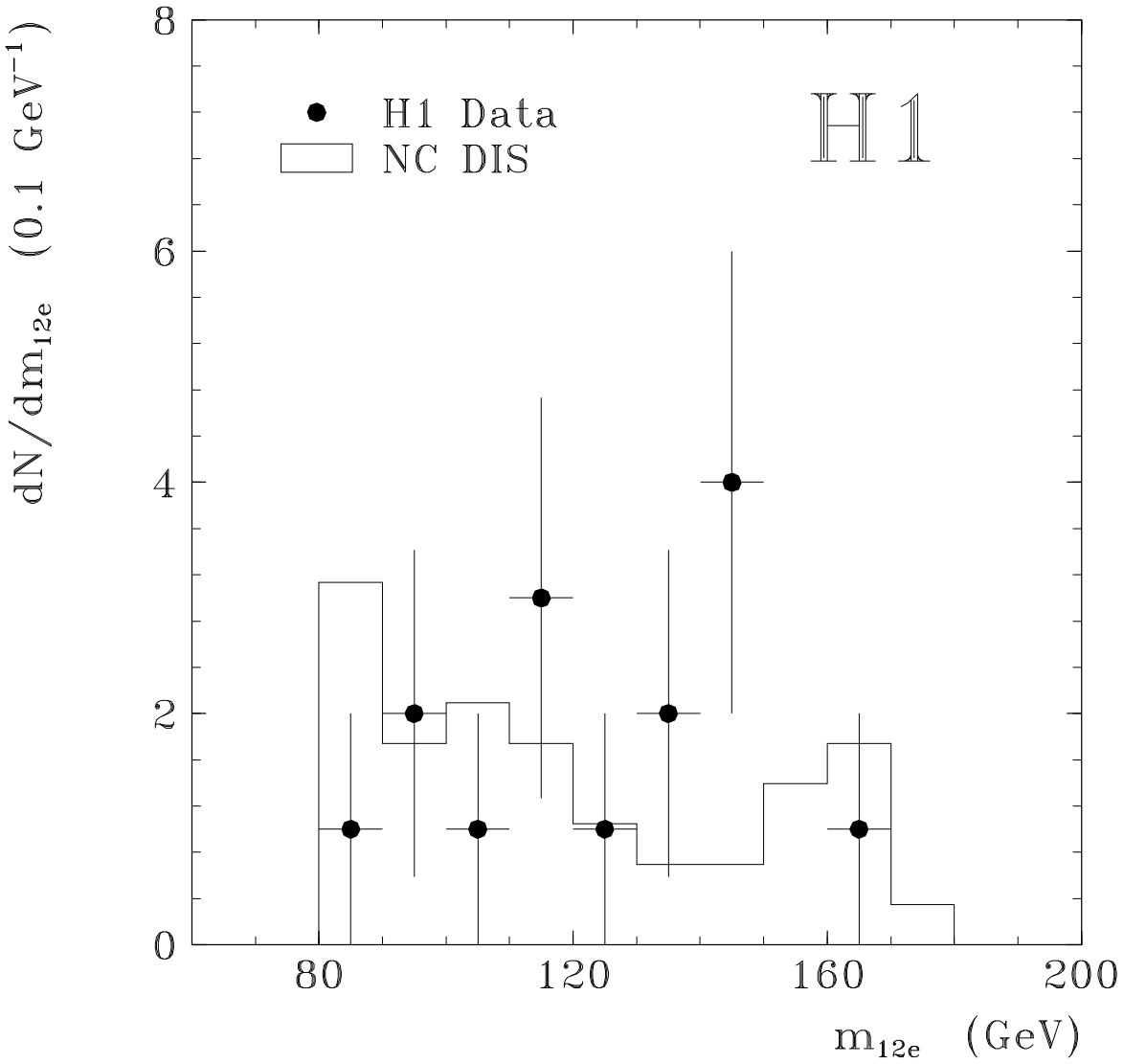

Figure 3: Mass spectrum of the selected electron and two jets. The histogram shows the absolute prediction based on the NC DIS Monte Carlo simulation.

In the following the uncertainties of the limits on $\sigma \cdot BR^*$ for the channel $e^* \to e\gamma$ are discussed. The wiggles are due to possible statistical fluctuations of the number of candidate events. The other decay channels have fewer candidate events and therefore little or no fluctuations of the calculated limits. The uncertainties due to efficiency and integrated luminosity are similar for all channels.

A shift of the calorimeter energy scale by $\pm 5\,\%$ effectively shifts both the event masses and the resulting limits by approximately $\pm 5\,\%$ on the horizontal axis. A variation of sensitive energy cuts in the analysis by $\pm 5\,\%$ leads to statistical limit fluctuations of 5–10 % for e^* masses below 100 GeV, and has no effect for higher e^* masses.

The statistical uncertainty on the background estimator of 10 % in the lowest mass bin, the error in the knowledge of the total efficiency (2–3 %), and the error in the integrated luminosity (1.5 %) lead to a 15 % limit variation for e^* masses below 100 GeV, which decreases to 3.3 % at high e^* masses, where no candidates were found. In addition the use of other parton density parameterizations leads to variations in the derived limits of up to 10%.

Decay channel		Mass ℓ^*/GeV								
		25	50	75	81	92	100	150	200	250
$e^* \to e\,\gamma$		46	73	83	—	—	91	90	88	89
$e^* \to e\,Z$,	$Z \to e\,e$					67	63	84	82	75
$e^* \to e\,Z$,	$Z \to \mu\,\mu$					53	55	54	31	23
$e^* \to e\,Z$,	$Z \to \nu\,\nu$					0	0	84	87	80
$e^* \to e\,Z$,	$Z \to q\,\bar{q}$					2	27	77	69	64
$e^* \to \nu\,W$,	$W \to e\,\nu$				80	—	82	79	82	79
$e^* \to \nu\,W$,	$W \to \mu\,\nu$				28	—	30	11	4	6
$e^* \to \nu\,W$,	$W \to q\,\bar{q}'$				0	—	8	64	55	44
$\nu^* \to \nu\,\gamma$		13	24	47	—	—	58	60	61	71

Table 6: Total analysis efficiencies for different decay channels of the excited leptons. Efficiencies are given as percentages and are based on 200 simulated Monte Carlo events for each entry of the table, from which an absolute efficiency error of 2–3 % follows. An entry '—' means that no events were generated at this mass.

Using the specific model for excited leptons of Hagiwara et al. [2] one can also calculate limits on the quantity $c/\Lambda \cdot \sqrt{BR^*}$, where the coupling constant $c \equiv c_{\gamma e^* e}$ for e^* and $c \equiv c_{W \nu^* e}$ for ν^*. For the channel $e^* \to e\,\gamma$ and e^* masses of 50 GeV, 100 GeV, ..., 250 GeV the corresponding limits (in TeV^{-1}) with 95 % CL are 1.21, 0.97, 1.34, 2.45, and 11.1. For a typical value $c^2_{\gamma e^* e} = 1/4$ and an e^* mass of 100 GeV we currently rule out compositeness scale parameters $\Lambda < 440$ GeV.

The ν^* production cross section is very much suppressed in positron proton collisions compared to electron proton collisions due to the different charge of the exchanged W boson and the different quarks probed inside the proton. A derivation of an exclusion limit for Λ is only meaningful if the total width of the excited fermion is small compared to its mass. In the model of Baur, Spira and Zerwas [3] the decay of an excited neutrino into $\nu\gamma$ is allowed if the couplings f, f' are set to $1, -1$, which results in $c^2_{\gamma \nu^* \nu} = 1/4$. With this choice of parameters $\Lambda < 19.5$ GeV is excluded at a mass of 135 GeV where the total width already reaches 28 GeV. For a ν^* mass of 100 GeV compositeness scale parameters $\Lambda < 51$ GeV are ruled out by this experiment.

Searches for excited leptons are also performed in e^+e^- annihilation experiments [18]. At present the results obtained are restricted to masses below $\sim$ 135 GeV, however with better limits on the coupling than achieved in this experiment. The L3 collaboration e.g. quotes limits (95 % CL) on $c_{\gamma e^* e}/\Lambda \cdot \sqrt{BR^*}$ which range between 0.32–0.51 TeV^{-1} for e^* masses from 90–130 GeV.

4 Search for excited quarks

4.1 Cluster and jet analysis

As mentioned in the introduction the q^* production is dominated by γ exchange with very small values of the squared momentum transfer and the scattered positron is nearly always unseen in the detector. So the final state of $q^* \to q\,\gamma$ events is characterized by an isolated electromagnetic cluster with large transverse energy, E_t, and a jet which balances this E_t. Therefore the main backgrounds which could mimic the signal are NC DIS events for which the electron track is lost (mismeasured), WAB events with the electron identified as a jet, and photoproduction events with a high E_t jet having a large enough electromagnetic component to simulate a photon, or

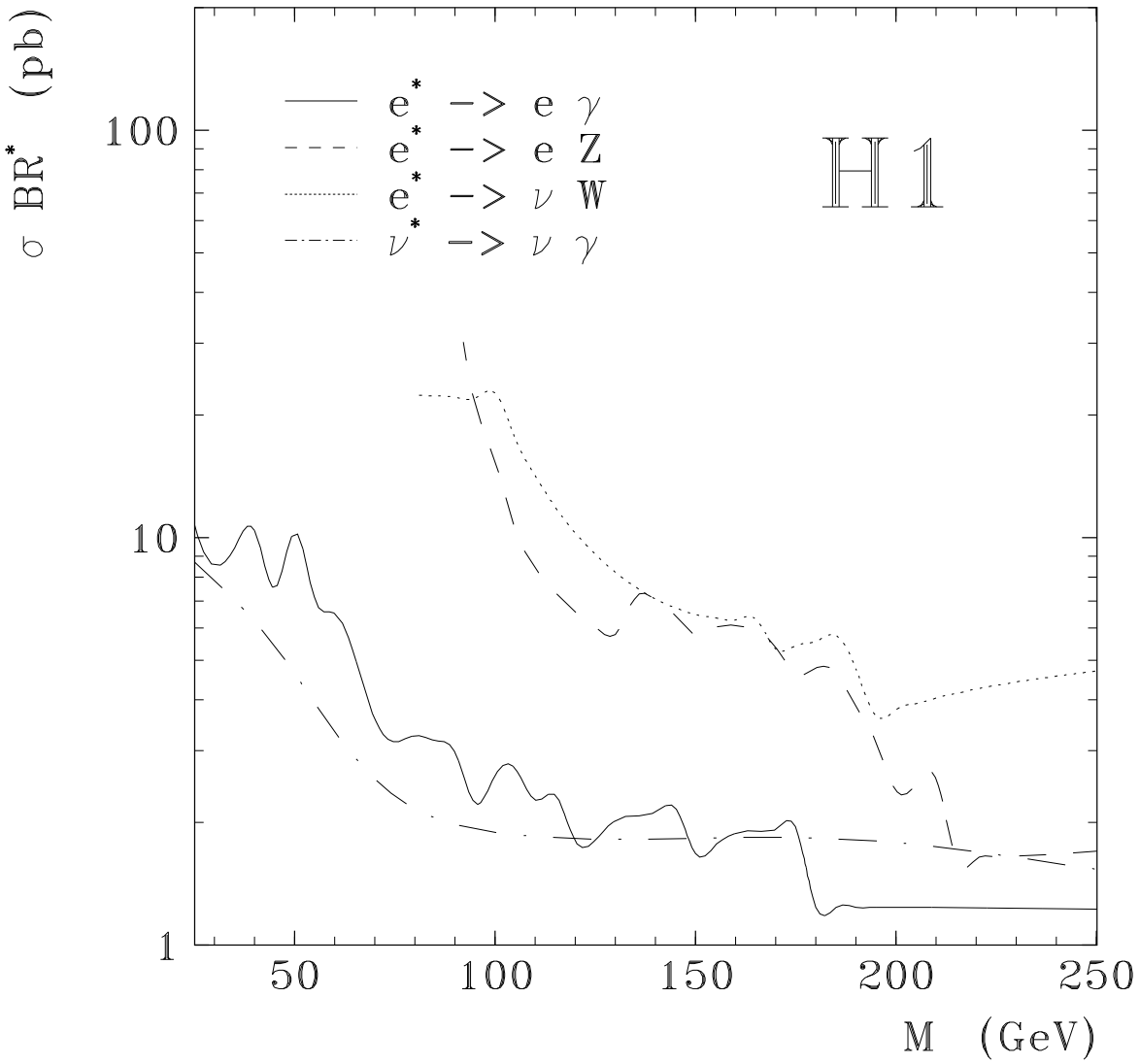

Figure 4: Rejection limits with a CL of 95% for e^* and ν^*. Regions above the curves are excluded. Decay channels of the heavy gauge bosons W and Z are combined.

1. ≥ 1 isolated e.m. cluster, $E_{t\gamma} > 20$ GeV
2. $20° < \theta_\gamma < 160°$
3. No track pointing to the e.m cluster
4. No electron candidate
5. ≥ 1 jets, $\Delta p_{x,y} < 3\sigma$
7. z-vertex must be reconstructed
8. Visual scan

Table 7: Selection requirements for the cluster and jet analysis. The variables are explained in the text. If more than one isolated electromagnetic cluster is found, that with the largest transverse energy is used as the photon candidate. The jet giving the best balance to the photon in transverse energy is used.

with the production of a prompt photon. The cuts to select candidates for the channel $q^* \to q\,\gamma$ are shown in table 7.

Requirements 1 to 3 are the basic selection cuts for photon candidates. The photon is taken as the highest E_t electromagnetic shower found in the LAr calorimeter with no corresponding track, i.e. no vertex-fitted track within a cone of $R = \sqrt{(\eta_{tr} - \eta_{em})^2 + (\phi_{tr} - \phi_{em})^2} < 0.3$ around the electromagnetic cluster center and no non-vertex-fitted central track with a projection on the front face of the calorimeter closer than 10 cm to the electromagnetic cluster center. These cuts reject most of the NC DIS events.

An independent search for electrons is then performed (requirement 4). Events with both a photon and an electron are rejected. This criterion mainly rejects WAB events and NC DIS events with wide angle final state radiation.

For the definition of the jets a cone algorithm with radius $R = 1$ in the η-ϕ-plane is used. At least one jet is requested (requirement 5). In the case of more than one jet being found, the jet which gives the best E_t balance to the electromagnetic cluster is kept. A 3σ p_x and p_y balance cut is then applied. This last selection is mass dependent and for each event the value of σ is chosen according to the invariant mass of the photon-jet-system. The dependence of the Δp_x and Δp_y distributions widths on the q^* mass has been determined using Monte Carlo events generated with such a q^* decay.

After applying all selection cuts, 8 candidates for $q^* \to q\,\gamma$ are found. A visual inspection of these candidates allows a clear interpretation of 6 of them : 5 are NC DIS with the electron track badly reconstructed and one is a photoproduction event.

For the background estimation, the generated NC DIS Monte Carlo events, corresponding to an integrated luminosity of 26.9 pb^{-1}, the WAB events [19] (18.4 pb^{-1}) and the photoproduction events (resolved: 3.72 pb^{-1}, direct: 4.04 pb^{-1}, direct with charm: 4.12 pb^{-1}) are all passed through the H1 detector simulation program and are subject to the same reconstruction and analysis procedure as the real data. The expected number of events from these different background processes, normalized to the integrated luminosity of 2.75 pb^{-1}, are 4.03 ± 1.12, 1.25 ± 0.65 and 2.04 ± 1.18 respectively. The quoted errors include statistical errors and an error of 1.5 % on the integrated luminosity . The invariant mass of the photon-jet-system of the 8 events is shown on Figure 5. The experimental mass resolution varies from 3.5 to 10 GeV for a q^* mass between 50 to 250 GeV. The absolute number of the events and the shape of the distribution are well described by the Monte Carlo simulation.

4.2 Results of q^* search

No model assumption is made in the search for a q^* decaying into a quark and a photon. However, in order to give limits on cross sections, specific assumptions are used to determine the detection efficiency for $q^* \to q\gamma$ events. The Monte Carlo event generator COMPOS [14] is used with the Lund string model giving fragmentation and decays and the MRS H [16] parameterization of parton densities. The generated events are then passed through the full H1 detector simulation and reconstructed in the same manner as the real data. The total detection efficiency is shown in table 8, as a function of the q^* mass.

Finally the 95 % CL rejection limit on $\sigma(q^*) \cdot BR(q^* \to q + \gamma)$ is shown in figure 6 as a function of the q^* mass. Cross sections above a value of about 9 pb for a q^* mass of 50 GeV down to a value of 2 pb for a q^* mass of 250 GeV are ruled out at the 95 % CL.

A variation of ± 2 % on the electromagnetic and ± 5 % on the hadronic energy scale of the LAr calorimeter corresponds to a systematic error on the limit which decreases from $+35$ % for

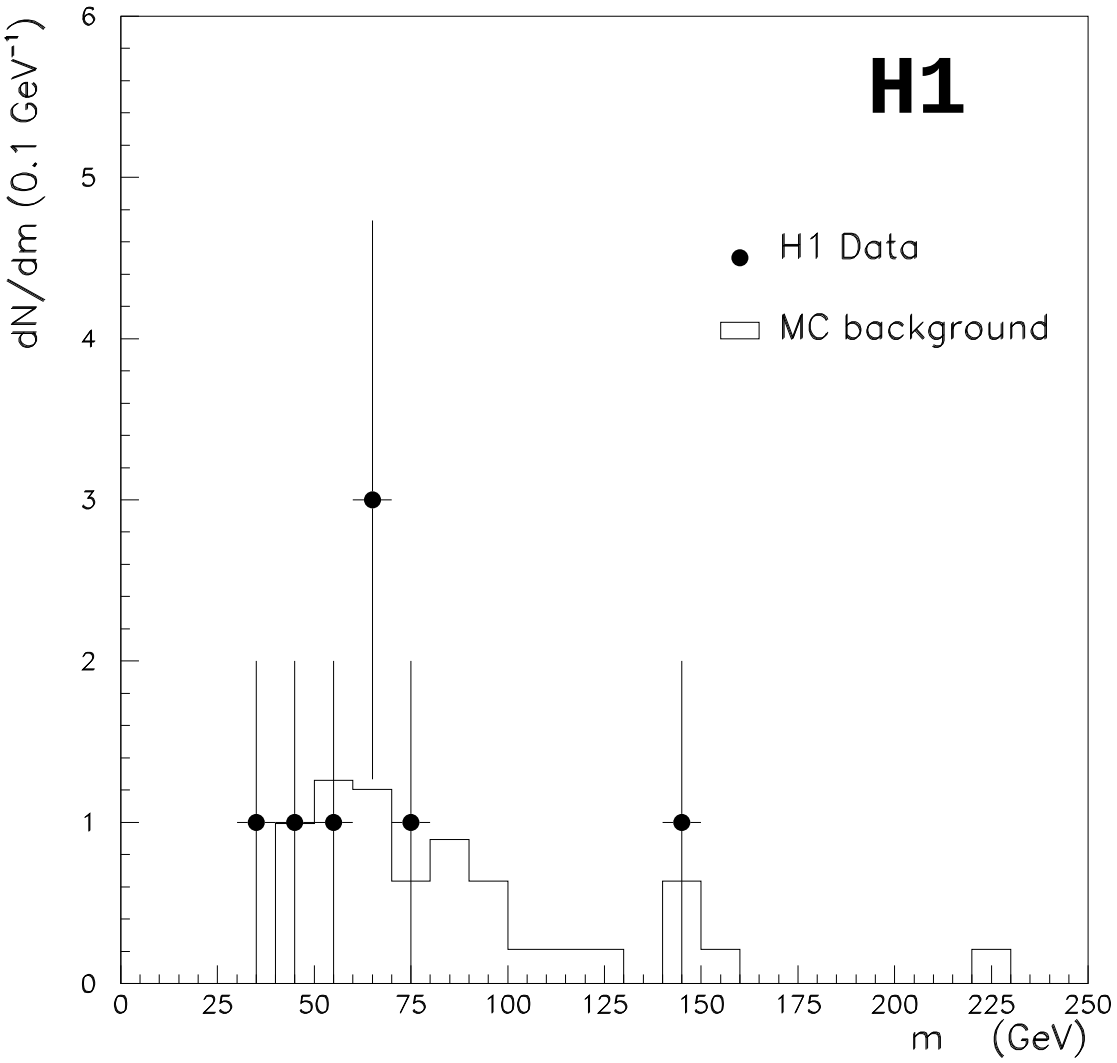

Figure 5: Invariant mass spectrum of the photon-jet-system. The points correspond to the data and the histogram to the background expectation.

	Mass q^*/GeV					
Decay channel	50	75	100	150	200	250
$q^* \to q\,\gamma$	30	47	50	55	49	53

Table 8: Total detection efficiency, given as a percentage based on 1000 simulated Monte Carlo events for each mass.

a q^* mass of 50 GeV (due mainly to a larger rejection rate with the p_t selection), to 10 % for a q^* mass above 75 GeV.

To determine the influence of the specific model used in computing detection efficiencies, we have simulated an isotropic angular decay distribution by re-weighting the COMPOS events.

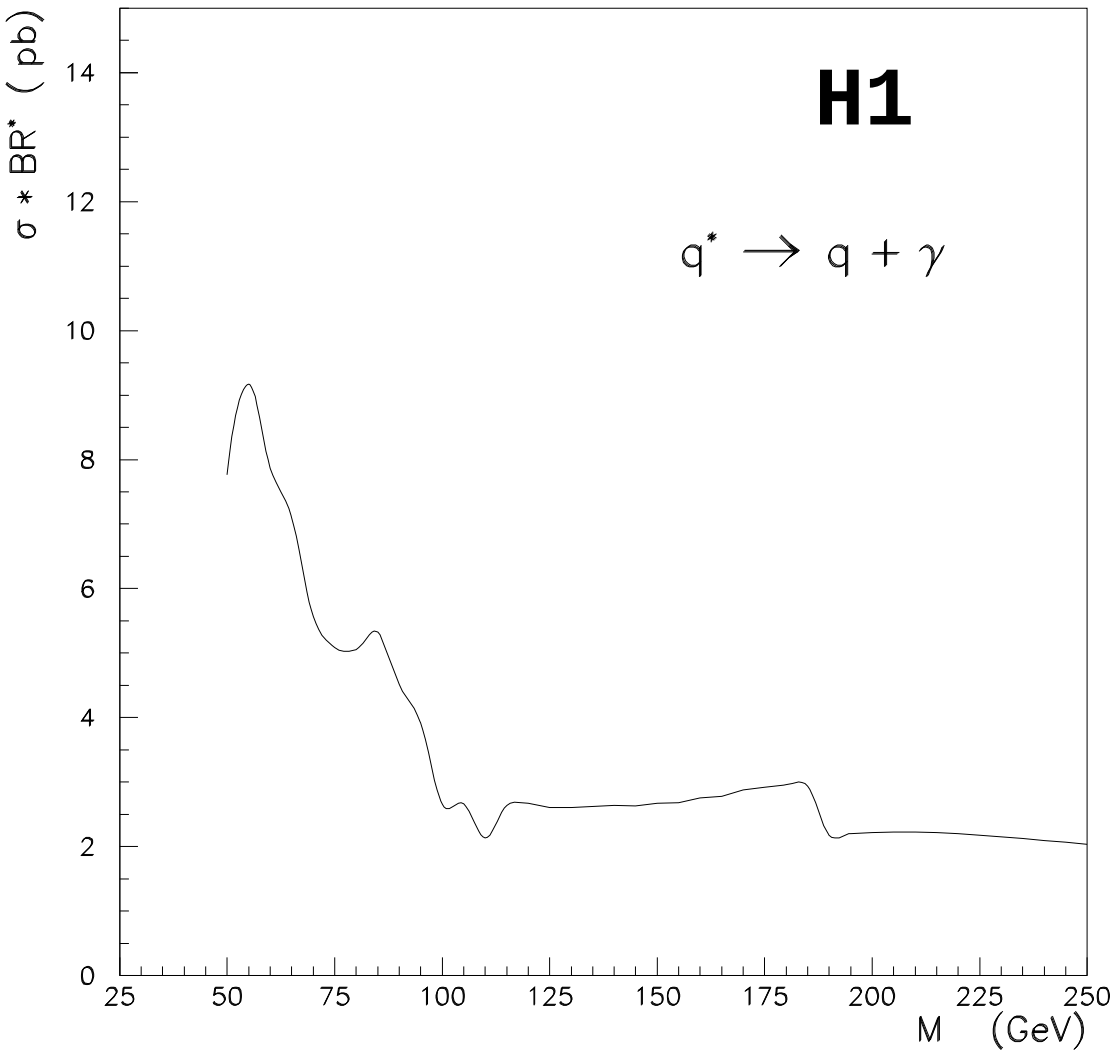

Figure 6: Rejection limit with a CL of 95 % on $\sigma(q^*) \cdot BR(q^* \rightarrow q + \gamma)$. The region above the curve is excluded.

The efficiency for finding the signal decreases from 19 % to 33 % for a q^* mass in the range 50–250 GeV. This would correspond to the limit for $\sigma(q^*) \cdot BR(q^* \rightarrow q + \gamma)$ varying from 11 to 3 pb.

Assuming a specific model [3] our limit can be transformed into a limit on the compositeness scale, Λ. However, this limit is strongly dependent on the relative coupling of $q^* \rightarrow qV$ (where V stands for γ Z W) to $q^* \rightarrow qg$. As an example, for a q^* mass of 100 GeV the limit on Λ goes from about 60 GeV (if the BR($q^* \rightarrow qg$) $\simeq$ 95%) to 290 GeV (if the BR($q^* \rightarrow qg$) $\simeq$ 25%). Our results are complementary to a search in proton anti-proton collisions [20] which investigates q^* production via quark gluon excitation.

5 Conclusions

Using data taken in 1994 new limits for the production of excited electrons in high energy electron proton interactions have been obtained. For excited electrons the search includes the decay channels $e^* \to e\gamma$, $e^* \to eZ$ and $e^* \to \nu W$, with the heavy bosons decaying into leptons or jets. New limits extending up to masses of 250 GeV are obtained. A search for excited neutrinos is also included considering only electromagnetic decays. In addition new limits for q^* production via electromagnetic excitation and decay are presented which complement results obtained at hadron colliders.

Acknowledgments We are grateful to the HERA machine group whose outstanding efforts made this experiment possible. We appreciate the immense effort of the engineers and technicians who constructed and maintain the H1 detector. We thank the funding agencies for financial support. We acknowledge the support of the DESY technical staff. We wish to thank the DESY directorate for the support and hospitality extended to the non-DESY members of the collaboration.

References

[1] F. Low, Phys. Rev. Lett. 14 (1965) 238.

[2] K. Hagiwara, S. Komamiya and D. Zeppenfeld, Z. Phys. C29 (1985) 115.

[3] U. Baur, M. Spira and P. Zerwas, Phys. Rev. D42 (1990) 815.

[4] B. Kniehl, Phys. Lett. B254 (1991) 267.

[5] H1 Collaboration, I. Abt et al., Nucl. Phys. B396 (1993) 3.

[6] H1 Collaboration, T. Ahmed et al., Phys. Lett. B340 (1994) 205.

[7] ZEUS Collaboration, M. Derrick et al., Z. Phys. C65 (1995) 627.

[8] H1 Collaboration, The H1 detector at HERA, DESY preprint 93-103 (July 1993); Internal Report, DESY H1-96-01 (March 1996) (to be published in NIM).

[9] F. Raupach, in proceedings Physics at HERA, Eds. W. Buchmüller, G. Ingelman, DESY Hamburg 1991, vol. 3, p. 1473.

[10] S.P. Baranov, O. Dünger, H. Shooshtari, J.A.M. Vermaseren, in proceedings Physics at HERA, Eds. W. Buchmüller, G. Ingelman, DESY Hamburg 1991, vol. 3, p. 1478.

[11] W.T Eadie, D. Drijard, F.E James, M. Roos and B. Sadoulet , Statistical Methods in Experimental Physics. North Holland Amsterdam and London, 1971 , p269.

[12] G. Ingelman, (LEPTO version 6.1), program manual unpublished; H. Bengtsson, G. Ingelman and T. Sjöstrand, Nucl. Phys. B301 (1988) 554.

[13] T. Sjöstrand, in proceedings Physics at HERA, Eds. W. Buchmüller, G. Ingelman, DESY Hamburg 1991, vol. 3, p. 1405, and references therein.

[14] T. Köhler, in proceedings Physics at HERA, Eds. W. Buchmüller, G. Ingelman, DESY Hamburg 1991, vol. 3, p. 1526

[15] B. Andersson, G. Gustafson and T. Sjöstrand, Phys. Lett. B94 (1980) 211; B. Andersson et al., Phys. Rep. 97 (1983) 31.

[16] A.D. Martin, W.J. Stirling, R.G. Roberts, Proceedings of the Workshop on Quantum Field Theoretical Aspects of High Energy Physics, Eds. B. Geyer, E.M. Ilgenfritz (1993) p. 11.

[17] K. Hikasa et al., Particle Data Group, Phys. Rev. D45 (1992) part II; H. Mönch, PITHA 91/2, thesis RWTH-Aachen (1991).

[18] ALEPH Collaboration, D. Buskulic et al., preprint CERN-PPE/96-087
DELPHI Collaboration, P. Abreu et al., preprint CERN-PPE/96-60
L3 Collaboration, M. Acciarri et al., Phys. Lett. B370 (1996) 211.
OPAL Collaboration, G. Alexander et al., preprint CERN-PPE/96-094

[19] A. Courau, S. Kermiche, T. Carli, P. Kessler, in proceedings Physics at HERA, Eds. W. Buchmüller, G. Ingelman, DESY Hamburg 1991, vol. 2, p. 902.

[20] CDF Collaboration, F. Abe et al., Phys. Rev. Lett. 74 (1995) 3538.